A stress-responsive p38 signaling axis in choanoflagellates

Florentine U.N. Rutaganira*[1], Maxwell C. Coyle[2,3], Alex P. Scopton[4], Arvin C. Dar[4], and Nicole King[2]

1. Departments of Biochemistry and Developmental Biology, Stanford University School of Medicine, Stanford, CA, 94305
2. Howard Hughes Medical Institute and the Department of Molecular and Cell Biology, University of California, Berkeley, CA, 94720
3. Current Institution: Department of Molecular and Cellular Biology, Harvard University, Cambridge, MA, 02138
4. Department of Oncological Sciences, Tisch Cancer Institute, Icahn School of Medicine at Mount Sinai, New York, NY, 10029

*Corresponding author: funr@stanford.edu

Abstract

Animal kinases regulate cellular responses to environmental stimuli, including cell differentiation, migration, survival, and response to stress, but the ancestry of these functions is poorly understood. Choanoflagellates, the closest living relatives of animals, encode homologs of diverse animal kinases and have emerged as model organisms for reconstructing animal origins. However, efforts to study kinase signaling in choanoflagellates have been constrained by the limitations of currently available genetic tools. Here we demonstrate that small molecule approaches provide a complementary and scalable approach for studying kinase function in choanoflagellates. To study the physiological roles of choanoflagellate kinases, we established two high-throughput platforms to screen the model choanoflagellate *Salpingoeca rosetta* with a curated library of human kinase inhibitors. We identified 95 diverse kinase inhibitors that disrupt *S. rosetta* cell proliferation. By exploring structure-activity relationships of one inhibitor, sorafenib, we identified a p38 kinase as a regulator of heat and oxidative stress in *S. rosetta*. This finding indicates a conserved p38 function between choanoflagellates, animals, and fungi. Moreover, this study demonstrates that existing kinase inhibitors can serve as powerful tools to examine the ancestral roles of kinases that regulate modern animal development.

Introduction

Phenotypic screens with libraries of small molecules have revolutionized cell biology by providing chemical tools to study protein function [1–4]. Because aberrant kinase activity leads to human disease [5,6], many tools have been developed to inhibit kinase activity and detect protein phosphorylation. Small molecules that target the kinase active site coupled with assays of kinase inhibition have uncovered effective therapeutic strategies to counter the functions of misregulated kinases, including inhibition of aberrant cell growth and proliferation caused by oncogenic kinases [5,7].

We sought to test whether kinase-regulated physiology in choanoflagellates, the closest living relatives of animals, could be revealed by kinase inhibitors. Choanoflagellates possess homologs of diverse animal kinases (Figure S1) [8–10] and, due to their phylogenetic placement, are well-suited for studies of the ancestral functions of animal cell signaling proteins [11,12].

Although targeted genome editing has been established in choanoflagellates [13], we inferred that the unique strengths of small molecules, including precise temporal control and discrete inhibition of enzymatic activity [14], might more readily reveal the physiological relevance of kinases, including those with essential functions, in choanoflagellates. Indeed, a previous study showed that two broad-spectrum kinase inhibitors disrupt cell proliferation in the choanoflagellate *Monosiga brevicollis* [15], but did not demonstrate whether kinases were directly targeted or identify specific pathways regulated by kinase signaling.

Using a library of well-characterized kinase inhibitors that vary in their human kinase inhibition profile, we treated cultures of *Salpingoeca rosetta*, a model choanoflagellate, in a multiwell format. We found that treatment of *S. rosetta* cultures with a set of kinase inhibitors disrupted cell proliferation and led to global inhibition of *S. rosetta* phosphotyrosine signaling. Using one of

these inhibitors, sorafenib, as a probe and inactive analogs as negative controls, we found that an *S. rosetta* p38 kinase homolog is activated by environmental stressors and signals downstream of sorafenib-inhibited kinases.

Results

Screening of a human kinase inhibitor library reveals small molecules that inhibit S. rosetta *kinase signaling and cell proliferation*

To investigate whether kinase activity regulates *S. rosetta* cell proliferation, we treated *S. rosetta* cultures with characterized human kinase inhibitors. Because the highest conservation between choanoflagellate and human kinases occurs in the kinase domain [8–10], we focused on kinase inhibitors that bind in the kinase active site. As a proof-of-concept, we first assayed staurosporine, a well-characterized broad-spectrum kinase inhibitor and inducer of cell death in diverse organisms [16,17]. Our initial screen used flow cytometry to measure the density of *S. rosetta* cells individually treated with staurosporine in multiwell plates. Staurosporine significantly and reproducibly reduced *S. rosetta* cell density (Figure S2A-C) and tyrosine phosphorylation (Figure S2D) in a dose-dependent manner.

After validating our flow cytometry pipeline with staurosporine, we expanded our study to screen 1255 inhibitors of diverse human kinases (Figure S1, Table S1). We screened *S. rosetta* cultures with each of the molecules in the library at 10 μM and measured cell density at a 24-hour endpoint (Figure 1A, Figure 1B, Table S1). This screen revealed 44 compounds (3.5% of the library) (Figure 1A and Figure S3) that significantly decreased *S. rosetta* cell counts compared to DMSO controls.

As a secondary assay, we pursued an imaging-based workflow to measure cell number. Although *S. rosetta* cell counts could be measured by flow cytometry without staining reagents, our co-culture system and treatment paradigm presented two potential sources of inaccuracy: compound aggregation due to low solubility in choanoflagellate media and choanoflagellate-sized clumps of bacterial biofilm. Therefore, we developed an imaging pipeline to enumerate *S. rosetta* cells by segmenting fixed-cell immunofluorescence micrographs at a 48-hour endpoint. Our imaging pipeline was able to distinguish wells with staurosporine-treated cells from DMSO controls (Figure S2E, F) with comparable z' standard statistics to flow cytometry (Figure S2B, S2E) [18]. This orthogonal approach identified 22 compounds (1.8% of the library) that overlapped with the flow cytometry screen and 51 additional molecules (4.4% of the library) that inhibited *S. rosetta* cell proliferation but were not identified in our flow cytometry screen (Figure 1A, Figure 1C, Figure S2G, Figure S3). In total, both screens identified 95 ATP-competitive inhibitors of human protein and lipid kinases (Figure S4A-C) that ranged in selectivity (Figure S4D).

Our strategy of using two complementary screening approaches uncovered human kinase inhibitors that interfere with *S. rosetta* cell proliferation. Choanoflagellates are predicted to express kinases that regulate animal cell growth, including mitotic kinases [19], the serine-threonine kinase Akt [20], and a diverse set of tyrosine kinases [8]. We identified GSK461364 and Volasertib, inhibitors of polo-like kinase 1 (PLK1), a mitotic kinase, in both screens (Figure S3). In addition, both screens identified diverse inhibitors of human Akt and tyrosine kinases (Figure S3). We also identified inhibitors of *S. rosetta* cell proliferation that disrupt human kinase signaling indirectly, i.e. without binding to a kinase (Figure S3). For example, genistein, a natural product that indirectly alters kinase activity [21,22], inhibited *S. rosetta* cell proliferation and was previously shown to inhibit the growth of the choanoflagellate *M. brevicollis* [15].

Some inhibitors of* S. rosetta *cell proliferation also disrupt* S. rosetta *phosphotyrosine signaling

After identifying human tyrosine kinase inhibitors that inhibited *S. rosetta* cell proliferation in our screens, we used biochemical methods to determine if the phenotype observed was correlated with inhibition of *S. rosetta* kinase activity. Widely available commercial phospho-specific antibodies that distinguish phosphorylated amino acids can reveal kinase activity in diverse organisms [15,23–26] and have been used to detect tyrosine phosphorylation by heterologously expressed choanoflagellate kinases [27–30]. We triaged our set of 95 identified proliferation inhibitors to focus on those compounds that inhibit human tyrosine kinases (e.g. tyrosine kinase inhibitors, multi-class targeting kinase inhibitors) (Figure S3), as opposed to those that inhibit serine or threonine phosphorylation, due to the relative lack of specificity of commercially-available phosphoserine and phosphothreonine antibodies [24–26].

In particular, we focused on four inhibitors – sorafenib, glesatinib, masitinib and PP121 – that were identified by either or both screening paradigms (Table S1, Figure S3) and have a narrower range of kinase targets than staurosporine [31–34]. In humans, sorafenib, glesatinib, masitinib and PP121 inhibit select receptor tyrosine kinases (RTKs). Masitinib and PP121 also inhibit Src kinase and PP121 additionally inhibits PI3K [31–33]. Specific residues shared in the kinase domains of human and choanoflagellate tyrosine kinases suggested that these inhibitors might effectively inhibit choanoflagellate tyrosine kinases. For example, choanoflagellate tyrosine kinases have residues within the predicted active site that are necessary for kinase activity in other organisms (e.g. “K” in VAIK, “D” in HRD and DFG) (Figure S5A) [8,35–37] and additional residues that confer sensitivity towards tyrosine kinase inhibitors (Figure S5B-D) [38,39].

Of the four inhibitors tested, *S. rosetta* cultures were most sensitive to sorafenib and glesatinib. Although 1 μM masitinib and PP121 were sufficient to reduce *S. rosetta* cell proliferation over the first 40 hours of treatment (Figure 2A), masitinib- and PP121-treated cultures recovered within 85 hours. In contrast, sorafenib and glesatinib inhibited cell proliferation throughout the 85-hour growth experiment at 1 μM (Figure 2A) and decreased cell density at 1 μM and 10 μM (Figure 2B). Glesatinib treatment induced cell lysis (Movie S1), whereas sorafenib induced cell body elongation (Movies S2-S3), in comparison to DMSO control (Movie S4). Importantly, treatment of *S. rosetta* cultures with 1 μM sorafenib or glesatinib led to a global decrease in phosphotyrosine signal, while treatment with 1 μM masitinib or PP121 did not decrease phosphotyrosine levels as detected by western blot (Figure 2C).

These findings showed that some kinase inhibitors, including sorafenib and glesatinib, could disrupt both *S. rosetta* cell proliferation and tyrosine kinase signaling. To further investigate patterns among human kinase inhibitors that showed this effect and identify kinases that may be relevant for the observed inhibition, we tested a panel of 17 human TK inhibitors (Figure S6) that share overlapping kinase targets with sorafenib and glesatinib. Of the 17 compounds tested, treatment with four additional small molecules (regorafenib, AD80, milciclib, and vemurafenib) led to a global decrease in phosphotyrosine staining (Figure S6A, "*") but not phosphoserine and phosphothreonine staining (Figure S7) as detected by western blot. These four inhibitors mildly reduced the rate of cell proliferation (Figure S6B, Figure S8). Other tyrosine kinase inhibitors inhibited *S. rosetta* cell proliferation but did not inhibit phosphotyrosine signaling, including PP2 (Figure S6C, Figure S8), consistent with prior findings in *M. brevicollis* [15]. Together, these observations provide independent support for the hypothesis that select kinases regulate cell proliferation in choanoflagellates.

Sorafenib binds to* S. rosetta *p38 kinase

To identify specific *S. rosetta* kinases whose activity might regulate *S. rosetta* cell
135 proliferation, we focused on sorafenib, an inhibitor with well-characterized structure-activity relationships in animals. We started with a kinase-enrichment strategy previously used in animals and plants to enrich kinases out of prepared lysates [40,41]. We used ActivX ATP and ADP probes [40,41] to covalently enrich for kinases and high-affinity kinase-binders present within *S. rosetta* lysates after pretreatment with vehicle (DMSO) or sorafenib.

140 Because sorafenib and ActivX probes competitively bind to kinase active sites, kinases that were more often enriched with DMSO pretreatment and less enriched with sorafenib pretreatment were likely sorafenib binders. We quantified absolute protein abundance [42] and focused our attention on kinases that were present in both DMSO and sorafenib pretreated samples but were enriched in multiple DMSO replicates, represented by higher ProteinLynx
145 Global Server (PLGS) protein scores [42]. Through this approach, we identified a predicted *S. rosetta* p38 kinase (Figure S9A) that bound 10-fold less well to ActivX probe in the presence of sorafenib (Figure 3, Table S2). Hereafter, we refer to this protein as *Sr*-p38.

ActivX probes and other unbiased approaches have previously identified human p38 kinases as primary targets of sorafenib [43,44]. In animals, sorafenib preferentially binds kinases
150 with threonine gatekeeper residues [44], including tyrosine kinases and two of four vertebrate p38 kinase paralogs with threonine gatekeepers [44] (Figure S9A). *Sr*-p38, contains a threonine gatekeeper (Figure S9A) and lysine residues necessary for ActivX probe binding. Because sorafenib displaced ActivX probe binding to *Sr*-p38, we infer that sorafenib binds to *Sr*-p38.

155

***Kinases upstream of p38 kinase regulate cell proliferation in* S. rosetta**

To uncover the *in vivo* mechanism by which sorafenib inhibited *S. rosetta* cell proliferation, we compared the response of *S. rosetta* wild-type and p38-mutant cell lines to treatment with a panel of p38-selective human kinase inhibitors. In a previous study, two of four human p38 kinase paralogs with threonine gatekeepers, p38α and p38β bound less to skepinone-L, a p38-selective human kinase inhibitor, and sorafenib when the p38 threonine gatekeeper was mutated to methionine. We reasoned that if the sensitivity to p38 inhibitor binding was conserved in *Sr*-p38, and if *Sr*-p38 directly regulated cell proliferation in *S. rosetta*, *Sr*-p38^{T110M} mutant cell lines would lose sensitivity to sorafenib, skepinone-L and BIRB 796, another p38-selective human kinase inhibitor that more potently inhibits human p38α and p38β.

Sorafenib, skepinone-L and BIRB 796 reduced wild-type *S. rosetta* cell proliferation at 1 μM (Figure 4A) and almost entirely abrogated cell proliferation at 10 μM during an 80-hour growth course (Figure 4A). In addition, *S. rosetta* cells treated with skepinone-L showed a similar cell elongation response to sorafenib treatment (Movies S2, S3, S5). We generated two independent *Sr*-p38^{T110M} cell lines by isolating two clones from a population of cells that underwent CRISPR-mediated gene editing [13] to mutate ACA to ATG at codon 110 of *Sr-p38* (Figure 4B). Co-editing for cycloheximide (CHX) resistance was used to enrich for clones that were nucleofected with the Cas9 ribonucleoprotein and grew in the presence of cycloheximide, which is toxic to wild-type *S. rosetta* cells [13]. Both *Sr*-p38^{T110M} cell lines, CHX *Sr*-p38$^{T110M-1}$ and CHX *Sr*-p38$^{T110M-2}$, grew similarly to cycloheximide-resistant controls, CHX^{1} and CHX^{2}, (Figure 4C) and were not desensitized to sorafenib, skepinone-L or BIRB 796 treatment (Figure 4D). Thus, we concluded that sorafenib, in addition to binding directly to *Sr*-p38, independently inhibits kinases upstream of *Sr*-p38 and thereby decreases *S. rosetta* cell proliferation. Future studies will be required to identify additional binding targets of sorafenib.

180 ***Sorafenib inhibits the stress-responsive p38 kinase signaling axis conserved in* S. rosetta**

Because we did not find a direct connection between inhibition of *Sr*-p38 activity and inhibition of *S. rosetta* cell proliferation, we sought to identify an acute physiological role for *Sr-p38* that could be altered by sorafenib treatment. Phylogenetic analyses place the origin of p38
185 in the last common ancestor of animals and fungi [45]. Environmental stressors activate p38 kinases in animals and fungi [45–52] and p38 kinase is present in diverse choanoflagellates (Figure S9B). However, the roles of p38 kinase in choanoflagellate biology are unknown. Although a previous study identified a nutrient-sensitive protein in *M. brevicollis* with a molecular weight similar to p38 kinases [15], the identity and function of this protein were not directly studied.

190 We wondered if stressors relevant to choanoflagellates would activate *Sr*-p38 signaling. Some choanoflagellates, including *S. rosetta*, live in sun-lit water zones that undergo daily and yearly fluctuations in temperature and nutrients [53–55]. To investigate if *Sr*-p38 is activated in response to environmental stressors, we exposed *S. rosetta* cultures to heat shock and oxidative stress. When *S. rosetta* cells cultured at ambient temperature were subjected to heat
195 shock and oxidative stress, we observed an increase in *Sr*-p38 phosphorylation (Figure 5A, B). In animals, upstream dual-specificity kinases (MAP2Ks) activate p38 by phosphorylating the threonine and tyrosine of the “TGY” motif [50,56], and this phosphorylation is recognized by several phospho-specific antibodies (Figure S9C). Within 30 minutes of heat shock at 37°C, the phospho-p38 signal from at least two protein species increased relative to pre-treatment (Figure
200 5A). We also observed an increase in signal for at least one protein using the phospho-specific p38 antibody on cell lysates that were treated with 0.5M hydrogen peroxide (Figure 5B). Because *Sr*-p38 contains the diagnostic “TGY” motif, we infer that this antibody recognizes *Sr*-

p38. Thus, the connection between environmental stress and the activation of p38 kinase appears to be conserved between yeast, animals, and choanoflagellates [45].

Previous studies have connected phosphotyrosine signaling and p38 kinase activation in animals in response to multiple stimuli (e.g. growth factors, ultraviolet light) [50,57]. Sorafenib blocks this signaling axis by inhibiting p38 and upstream kinases (e.g. tyrosine kinases, dual-specificity kinases) [44,58]. To examine if the signaling axis between upstream kinases and p38 is conserved in *S. rosetta,* we tested whether sorafenib could reduce the observed phosphorylation of *Sr*-p38 in *S. rosetta* cultures subjected to heat shock. As a control, we used APS6-46, a sorafenib analog that shares sorafenib's core structure but has modifications that make it too large to bind to most sorafenib kinase targets [59]. APS6-46 does not inhibit *S. rosetta* tyrosine phosphorylation or cell division (Figure S10), and a previous study found that similar sorafenib analogs could control for off-target inhibition of non-kinase proteins by sorafenib [59]. *Sr*-p38 signaling was not activated in *S. rosetta* cultures pretreated with sorafenib, whereas cultures pretreated with APS6-46 (Figure 5C) or human p38 kinase inhibitors (Figure S11) retained *Sr*-p38 phosphorylation comparable to the DMSO control. Because sorafenib treatment blocked *Sr*-p38 activation and inhibited phosphotyrosine signaling, we infer that sorafenib blocks *Sr*-p38 signal transduction through inhibition of upstream kinases that transduce the heat and oxidative stress response in *S. rosetta* (Figure 5D).

Discussion

230 To investigate the relevance of kinase signaling in choanoflagellate physiology, we have established two high-throughput phenotypic screens of cells treated with a small molecule library. By treating *S. rosetta* cultures with validated human kinase inhibitors, we uncovered molecules that revealed the physiological relevance of kinases as regulators of *S. rosetta* cell proliferation. Moreover, we identified biologically relevant environmental stressors that activate
235 p38 kinase signaling in *S. rosetta*.

Until recently, the functions of stress-responsive kinases, including p38, JNK, and Hog1, were only characterized in animals and fungi [45]. However, this family of kinases evolved before the divergence of animals and fungi and expanded in choanoflagellates, which encode at least two paralogs [45]. Our discovery that *S. rosetta* phosphorylates proteins in response to heat and
240 oxidative shock (Figure 5A, B) demonstrates that choanoflagellates undergo stress-responsive signaling. Because the phosphorylation of these stress-activated proteins can be inhibited by sorafenib (Figure 5C), a known binder of animal p38 [44] and *Sr*-p38 (this study), we infer that *Sr*-p38 is an *S. rosetta* stress-responsive kinase.

Our approach of using sorafenib to uncover the role of Sr-p38 and sorafenib-targeted
245 kinases in *S. rosetta* allowed us to bypass potential limitations with genetic approaches. Vertebrates express four p38 paralogs; the p38α knockout is embryonic lethal, whereas knockouts for the other p38 paralogs are viable [50]. *S. rosetta* is predicted to encode at least two stress-responsive kinases, including *Sr*-p38 and EGD82769 (Figure S9), but it is unknown if they have independent functions. We observed multiple bands when subjecting *S. rosetta*
250 cultures to heat shock (Figure 5A), suggesting either that *Sr*-p38 exists in multiple isoforms or that the phospho-p38 specific antibody that is selective for the diagnostic p38 “TGY” motif found in *Sr*-p38 showed cross-reactivity with the EGD82769 “TPY” motif (Figure S9). Sorafenib

inhibited phosphorylation of both proteins (either isoforms of *Sr*-p38 or *Sr*-p30 and EGD82769) (Figure S9). The insensitivity of *Sr*-p38^{T110M} mutant cell lines (Figure 4D) to sorafenib suggests that the small molecule targets additional stress-responsive kinases.

Choanoflagellates have dynamic life histories and diverse kinase families, including p38 kinases, that are found in animals [8,10,19,45,60]. How kinases regulate additional aspects of choanoflagellate physiology, including life history transitions, remains to be investigated. We infer that fast-acting inhibition of kinase activity will be a powerful approach to study the roles of kinases that regulate cell state transitions in choanoflagellates. Because kinase inhibitors allow the enzymatic activity of kinases to be disrupted while preserving kinase localization and scaffolding functions, using small molecules as tools can distinguish whether kinase catalytic activity or other kinase functions are necessary for choanoflagellate development [14,61]. Insight into the roles of individual kinases during the emergence of new cell-cell signaling networks (e.g., receptor tyrosine kinase signaling in holozoans) will be fundamental to understanding the contributions of kinase signaling to the origin of animal multicellularity.

Materials and Methods

Supplementary Materials and Methods

Co-culturing of S. rosetta *with the prey bacterium* Echinicola pacifica

Choanoflagellates are bacterivores and require prey bacteria that are co-cultured in choanoflagellate media [62]. *Echinicola pacifica*, a Bacteriodetes bacterium, grown in seawater-based media enriched with glycerol, yeast extract, and peptone sustains *S. rosetta* growth [63]. This co-culture of *S. rosetta* and *E. pacifica*, publicly available from the American Type Culture Collection (ATCC) as ATCC PRA-390 and also known as “SrEpac” [63], was used in this study.

280 ***High-throughput chemical screening in* S. rosetta**

To quantify changes in *S. rosetta* cell proliferation after small molecule treatment, we established a high-throughput screening pipeline.

We first assembled a library of 1255 compounds (Table S1) from commercial (Selleckchem Kinase Inhibitor Library Catalog #L1200 Lot: Z1316458) and academic (Kevan M.
285 Shokat, University of California, San Francisco) sources. 98% of molecules in the library were characterized as human kinase inhibitors and 2% were compounds that are cytotoxic to other protists. Most of the kinase inhibitors in the library modulate human kinase activity by binding to the kinase active site and are ATP-competitive. Because we did not know if inhibitors designed to bind to human kinases would bind to choanoflagellate kinase homologs with the same
290 potency or selectivity, we chose inhibitors with a range of selectivity: 75% of the human kinome is targeted by at least one inhibitor in the library, and the library includes inhibitors of all classified human kinase groups (Figure S1). Compounds dissolved at 10 mM in dimethyl sulfoxide (DMSO, Sigma #D8418) were placed into individual wells of 384-well deep well master plates (Corning #3342). We generated deep well stock plates with solutions that could be
295 directly transferred to assay plates. Liquid handling (Agilent V11 Bravo) was used to dilute compound master plates (containing 10 mM compound in 100% DMSO) into deep well stock plates (containing 450 μM compound in 4.5% DMSO).

In a primary screen, *S. rosetta* cell counts were determined by analysis of acquired flow cytometry events after a 24-hour incubation. Assay plates were generated by plating 2 μL of the
300 deep well stock plates into 384-well assay plates (Thermo Scientific #142761 using the Agilent V11 Bravo). 88 μL of SrEpac cultured in high-nutrient media (5% Sea Water Complete) [64] at exponential phase (~$9x10^5$ cells/mL) was diluted to $2x10^4$ cells/mL in high-nutrient media and dispensed into the assay plate (ThermoFisher Mulitdrop™ Combi with long standard dispensing

tube cassette #24072677) to treat the SrEpac culture at 10 μM compound and 0.1% DMSO.
305 After a 24-hour incubation, assay plates were individually placed into an autosampler (BD Biosciences High Throughput Sampler, HTS) running in high-throughput mode. 40 μL of each well was mixed twice (at 180 μL/second), and 10 μL of cells from each well were loaded onto a flow cytometer (BD Biosciences LSR II) at 1 μL/second. In between each well, the autosampler needle was washed with 400 μL of sheath fluid (1X phosphate-buffered-saline pH 7.4). Loaded
310 cell samples were acquired on the cytometer with forward scatter (FSC) and side scatter (SSC) parameter voltages set to 538 and 308, respectively. A polygon gate from a DMSO well within a plate (D23 for Plate 1 and C23 for Plates 2-4 due to a shift in the distribution of observed events) was used to analyze events and quantify cell counts for all wells in an individual assay plate using FlowJo v10.8™ (BD Biosciences) (Figure S2A).

315 In a secondary screen, *S. rosetta* cell counts were determined by enumerating segmented cell objects from immunofluorescence images taken on an Opera Phenix high-content imager after a 48-hour incubation. Assay plates were generated by adding 4 μL of compound in the deep well stock plates into 96-well assay plates containing 176 μL of SrEpac in low-nutrient medium (1% Cereal Grass Medium and 1% Sea Water Complete [13]) using an
320 electronic multichannel pipetter (Rainin E4 Multi Pipette E8-20XLS+). Cells were initially expanded in high-nutrient media containing 4% Cereal Grass Medium and 4% Sea Water Complete [13] and at exponential phase (~$1x10^6$ cells/mL), diluted to $2x10^4$ cells/mL with AK-seawater. After a 48-hour incubation, cells were mixed in a thermomixer for two minutes at 800 rpm at room temperature to dislodge any cells attached to biofilm at the bottom of the 96-well
325 plate. 100 μL of cells were transferred to Poly-D-Lysine (Sigma # P6407) coated 384-well imaging plates (Perkin Elmer Cell Carrier Ultra Plates #6057302) using an electronic multichannel pipetter (Rainin E4 Multi Pipette Multi E12-200XLS+). To optimize the screen, after

40 minutes of adherence, 1 µL of FM 1-43X mixture (1 µL of 500 µg/mL mixture of FM1-43X dye made by dissolving tube in 200 µL of methanol) was added to the cells and incubated for 15 minutes. 50 µL of the cell dye-mixture was removed followed by fixation and washing as described next for the full screen. For the full screen, after 40 minutes of adherence, 50 µL of cells were removed, and the remaining 50 µL were washed once with 50 µL 4X PBS. After incubating in the 4X PBS for 5 minutes, 50 µL was removed. Cells were fixed for 20 minutes at room temperature by adding 50 µL of 4% formaldehyde in PEM buffer (100 mM PIPES pH 7, 1 mM EGTA, 1 mM $MgSO_4$). After fixation, cells were washed by removing 50 µL of solution from the plate and adding 50 µL of PEM buffer three times. After the final wash, 75 µL of solution was removed. At this point, cells for the optimization screen were imaged on a Perkin Elmer Opera Phenix with the following imaging specifications for the Fluorescein (FITC) channel: 20X water objective (NA 1.0, working distance 1.7mm, 646 μm^2 field of view), 60ms and a three plane zstack at -8µm, -6µm and -4µm. For the full screen, after washing the fixative, cells were blocked by adding 75 µL of 2% BSA and 0.6% Triton-X100 in PEM for 30 minutes at room temperature. After blocking 25 µL was removed and 25 µL of primary antibody solution in 1% BSA and 0.3% Triton-X100 in PEM was added to stain the cell body and flagella overnight at 4°C (anti-tubulin, Abcam #ab6161, 1:1000 dilution). Due to the amount of time required for imaging, plates were staggered and processed one plate each day. On each imaging day, a plate was brought to room temperature and the primary antibody was washed three times by adding 50 µL of 1% BSA and 0.3% Triton-X100 in PEM and removing 50 µL of solution from the plate three times. Secondary antibody (Goat anti-rat Alexa Fluor 488, Invitrogen #A-11006, 1:300 dilution) and nuclear stain (DRAQ5, Thermo Scientific #62251, 1:500 dilution) were added in 25 µL of 1% BSA and 0.3% Triton-X100 in PEM and incubated for 2 hours at room temperature. After incubation, the secondary antibody was washed three times by adding 50 µL of PEM and removing 50 µL of solution from the plate three times. To stain the cell collar and

obtain a second cell body marker, rhodamine phalloidin (Invitrogen #R415, 1:300 dilution) and Cell Tracker cmDIL (Invitrogen # C7000, 250 nM) were added for 25 minutes. To preserve the
355 staining, 50 µL of solution was removed from the plate and 50 µL of 50% glycerol in PEM was added. 22 fields of view in 4 planes (each plane separated by 1 µm) of each well in the 384-well plate were imaged with a 40X Water immersion objective (NA 1.1, working distance 0.62mm, 323 μm^2 field of view) on a Perkin Elmer Opera Phenix with optimized imaging specifications for each channel (Alexa 488 – Tubulin – 20ms; TRITC – Cell Tracker cmDIL / rhodamine phalloidin
360 – 100ms; Brightfield – 100ms; Alexa Fluor 647 – DRAQ5 / Nuclei – 1s). Due to restrictions on the available image area on the opera phenix, columns 1-23 of each 384-well plate were imaged first followed by a second scan with column 24 alone.

For both assays, the quantified cell counts were normalized to the average cell count of all DMSO wells within an individual plate to account for any plate-to-plate variation. Compounds
365 were determined to significantly inhibit *S. rosetta* cell proliferation if the resulting normalized cell count had a p-value < 0.05 (based on two-tailed p-value calculated from z-score of all treated samples). The resulting normalized cell count data were plotted using GraphPad Prism 9.3.1™ (GraphPad San Diego, California, USA) (Figure 1; Figure S2B-C, Figure S2E, Figure S2G).

Follow-up* S. rosetta *cell proliferation assays in response to compound treatment

370 Compound treatments post-library screening were conducted with commercially available inhibitors; sorafenib analogs previously synthesized [58]; AD80 previously synthesized [65]; and imatinib, PP1, and sunitinib provided by K. Shokat (UC San Francisco). Sorafenib (#S1040), regorafenib (#S5077), dasatinib (#S7782), PP2 (#S7008), and milciclib (#S2751) were purchased from Selleckchem. Glesatinib (#HY-19642A), masitinib (#HY-10209), lapatinib
375 (#HY-50898), PP121 (#HY-10372), gliteritinib (#HY-12432), brigatinib (#HY-12857), RAF265 (#HY-10248), vemurafenib (#HY12057), skepinone-L (#HY-15300), BIRB 796 (#HY-10320),

were purchased from MedChem Express. SU6656 (#13338) was purchased from Cayman Chemical. R406 (#A5880) was purchased from ApexBio Technlology.

SrEpac cultured in high-nutrient media (4% Sea Water Complete with 4% Cereal Grass) [13] in exponential phase (~$5x10^5$ - $9x10^5$ cells/mL) was diluted to lower density ($1x10^4$ cells/mL), and 1 mL or 100 µL of cells were plated into 24-well or 96-well multiwell plates (Corning #3526, Thermo Scientific #260251), respectively. Cells were treated with compound by adding 1 µL of a 1000X compound stock in DMSO to a well in the 24-well plate or adding 1 µL of a 100X compound stock in DMSO. Equal volumes of DMSO were added to vehicle control wells so (v/v%) DMSO in controls was the same as compound treated wells. At set timepoints, cells were harvested. For cell assays in 24-well plates, cells in the well were pipetted up and down to resuspend the well and the well contents were transferred to a 1.5 mL Eppendorf tube. Cells were fixed by adding 40 µL of 37% formaldehyde (methanol-stabilized, Sigma-Aldrich #252549). For 96-well plates, 1 µL of 37% formaldehyde was added to each well by using a multichannel pipette, and a pierceable aluminum plate seal (USA Scientific TempPlate® Sealing Foil) was added to cover the plate. The plate was vortexed at 2000rpm (24-well plates) or 3000rpm (96-well plates) in a plate vortexer (Eppendorf ThermoMixer C) to ensure equal fixation of cells in the well. Fixed cells were immediately counted or placed at 4°C for up to 2 weeks before counting. The cell density of sample timepoints along the full growth course was determined by analysis of micrographs taken on a Widefield microscope (Carl Zeiss AG Axio Observer.Z1/7, Oberkochen, Germany) [13], or brightfield imaging using a cell counter (Logos Biosystems LUNA-FL™). The resulting normalized cell density data at each timepoint was plotted using GraphPad Prism 9.3.1™ (GraphPad San Diego, California, USA) (Figure 2A; Figure 4A; Figure 4C; Figure S6B; Figure S10C). For comparisons between growth curves and phosphotyrosine signal (see *Assessment of* S. rosetta *kinase signaling by western blotting)* the area under the growth curve (AUC) was analyzed using GraphPad Prism 9.3.1™ (GraphPad San Diego, California, USA)

with baseline at Y=0 and minimum peak height > 10% above the baseline to maximum Y value (Figure S8; Figure S10B).

For dose-response assays, SrEpac cultured in high-nutrient media (5% Sea Water Complete [64] or 4% Sea Water Complete with 4% Cereal Grass [13]) in exponential phase (~$5x10^5$ - $9x10^5$ cells/mL) was diluted to lower density. Starting density used varied based on treatment length: for 24-hour treatments and less, cells were plated at $2x10^5$ cells/mL; for 24-48 hour treatments, cells were plated at $1x10^5$ cells/mL; and for 48+ hour treatments, cells were plated at $5x10^4$ cells/mL. Cell density was determined at the treatment endpoint using the same approach as the treatment growth curves described in the preceding paragraph. The resulting normalized cell density data at each dose was plotted using GraphPad Prism 9.3.1™ (GraphPad San Diego, California, USA). (Figure 1B; Figure 4D; Figure S10D)

Assessment of* S. rosetta *kinase signaling by western blotting

After compound treatment, the SrEpac culture was harvested and lysed to quantify protein abundance and immunoblotting by western blot. *S. rosetta* cells were harvested by centrifugation at 6,000g for five minutes in Falcon tubes in a swinging bucket centrifuge and transferred into 1.5 mL Eppendorf tubes and washed two times with 4X phosphate buffered saline (PBS, 6.2 mM potassium phosphate monobasic, 621 mM sodium chloride, 10.8 mM sodium phosphate dibasic) with centrifugation at 6,000g for 5 minutes in a fixed angle centrifuge at room temperature in between each wash. Cells were resuspended and lysed in digitonin lysis buffer (20 mM Tris pH 8, 150 mM potassium chloride, 5 mM magnesium chloride, 250 mM sucrose, 1 mM Pefablock® SC serine protease inhibitor (Sigma-Aldrich Cat# 76307), 8 mM digitonin, 1 mM dithiothreitol, 0.06 U/μL benzonase nuclease, 1X Roche PhosSTOP phosphatase inhibitor cocktail, 1X Roche cOmplete protease inhibitor cocktail) for 30 minutes. Lysed cells were spun at 18,000g for 15 minutes at 4°C and supernatants were isolated. Protein

concentration in supernatants was determined by Bradford assay. Samples were boiled in loading dye (LiCOR #928-40004) and equal protein amounts for each sample were loaded onto NuPAGE™ 4-12% Bis-Tris SDS-PAGE gels (Invitrogen Cat#s WG1402BOX, WG1403BOX, NP0335BOX, NP0336BOX). To resolve bands recognized by the phospho-p38 antibody (Promega #V1211), a NuPAGE™12% Bis-Tris SDS-PAGE gel (Invitrogen Fisher NP0349BOX) was used. PageRuler™ or PageRuler Plus™ prestained protein ladder (Thermo Scientific #26614 and #26620), EGF-stimulated A431 cell lysate control (Sigma Aldrich #12-302), and *E pacifica* control lysate (lysed as for *S. rosetta* cells) were added to wells and gels were run in Novex NuPAGE MES buffer (Invitrogen Cat# NP000202). Gels were transferred to 0.45 µm nitrocellulose (Bio-Rad) in Tris-Glycine Buffer (Bio-Rad #1610734) with 10% Methanol. After transfer, blots were stained with LI-COR Revert™ 700 and total protein imaged. After total protein was stained, blots were blocked with 5% bovine serum albumin in Tris buffered saline (TBS, 25 mM Tris, 150 mM sodium chloride) for 1 hour. Primary antibodies (see next paragraph) were added in TBS with Tween (0.1%) and left overnight. Blots were washed with TBS-Tween four times. LI-COR secondary IRDyes® were added in TBS-Tween at 1:10,000 dilution and incubated for 1 hour at room temperature. Blots were washed with TBS-Tween four times and imaged with LI-COR Odyssey® imager (Figure 2C; Figure 5A-C; Figure S2D; Figure S6A; Figure S7; Figure S9C; Figure S10E; Figure S11). Staining intensities were quantified with Image Studio Lite 5.2.5 (LI-COR, 2014) (Figure S2D; Figure S8; Figure S10B).

Primary antibodies for pY1000 (#8954), anti-phospho-Erk (anti-phospho p44/42 MAPK, 4370) anti-phospho(Ser/Thr)-Phe (#9631), anti-phosphotheronine (#9381) and anti-phosphothreonine-proline (#9391) were purchased from Cell Signaling Technology. Anti-phospho p38 MAPK (Anti-ACTIVE® p38, #V1211) was purchased from Promega. Anti-

450 phosphoserine (Rb X, #AB1603) was purchased from Millipore Sigma. Anti-alpha-tubulin (YOL 1/34, #ab6161) was purchased from Abcam.

ActivX Mass Spectrometry workflow to identify* S. rosetta *proteins that bind sorafenib

For all mass spectrometry experiments, SrEpac cultures were grown to a high density in
455 Pyrex baffled flasks without shaking. In tall necked flasks, cultures were grown in the maximum volume of culture media, and an aquarium pump was used to bubble air into the foam-plugged PYREX® Delong flask pierced with a serological pipette at a bubbling rate of approximately one bubble/second [66]. For wide 2.8L PYREX® Fernbach flasks, bubbling was not needed. *S. rosetta* cells were harvested by spinning in 200mL Nalgene conicals at 2000g for 10 minutes in a
460 swinging bucket centrifuge at room temperature to obtain cell pellets. Cells were first washed by resuspending cell pellets from four conicals in approximately 45 mL of 4X PBS, transferring cells to 50 mL Falcon tubes, and spinning at 2000g for 10 minutes in a swinging bucket centrifuge at room temperature. Cells were washed a second time by resuspending cells in ~15 mL of 4X PBS per 50 mL Falcon tube, transferring cells to 15 mL Falcon tubes, and spinning at 2000g for
465 10 minutes in a swinging bucket centrifuge at room temperature. Cells were then ready for the ActivX probe workflow.

For ActivX probe enrichment, cells were lysed and 500 µL of 5 mg/mL supernatants were obtained as previously described [41]. 20 mM of manganese chloride cofactor was added to the lysate and incubated for 5 minutes followed by the addition of 100 µM sorafenib or 1%
470 DMSO (vehicle control) and incubation for 10 minutes. 20 µM ActivX probe was added for kinase capture. Biotinylated proteins were captured using streptavidin beads in the presence of 6M urea / immunoprecipitation (IP) lysis buffer, and samples were washed with 6M urea / IP lysis buffer. Protein samples were provided to the University of California, Davis mass

spectrometry facility (https://cmsf.ucdavis.edu) on beads and underwent standard tryptic digestion with Promega ProteaseMAX™ Surfactant, Trypsin Enhancer. Briefly, samples were first reduced at 56ºC for 45 minutes in 5.5 mM DTT followed by alkylation for one hour in the dark with iodoacetamide added to a final concentration of 10 mM. Trypsin was added at a final enzyme:substrate mass ratio of 1:50 and digestion carried out overnight at 37ºC. The reaction was quenched by flash freezing in liquid nitrogen and the digest was lyophilized. Digest was reconstituted in 0.1% TFA with 10% acetonitrile prior to injection. For quantification of peptides within each sample, 500 fmol of Hi3 *E. coli* standard reagent ClpB (Waters, Milford, MA) was placed into each sample and injected with 1.0 ug of total digest. Each sample was run in triplicate.

The mass spectrometry instrument used to analyze the samples was a Xevo G2 QTof coupled to a nanoAcquity UPLC system (Waters, Milford, MA). Samples were loaded onto a C18 Waters Trizaic nanotile of 85 µm × 100 mm; 1.7 µm (Waters, Milford, MA). The column temperature was set to 45°C with a flow rate of 0.45 mL/min. The mobile phase consisted of A (water containing 0.1% formic acid) and B (acetonitrile containing 0.1% formic acid). A linear gradient elution program was used: 0–40 min, 3–40 % (B); 40-42 min, 40–85 % (B); 42-46 min, 85 % (B); 46-48 min, 85-3 % (B); 48-60 min, 3% (B). Mass spectrometry data were recorded for 60 minutes for each run and controlled by MassLynx 4.2 SCN990 (Waters, Milford, MA). Acquisition mode was set to positive polarity under resolution mode. Mass range was set form 50 – 2000 Da. Capillary voltage was 3.5 kV, sampling cone at 25 V, and extraction cone at 2.5 V. Source temperature was held at 110C. Cone gas was set to 25 L/h, nano flow gas at 0.10 Bar, and desolvation gas at 1200 L/h. Leucine–enkephalin at 720 pmol/µl (Waters, Milford, MA) was used as the lock mass ion at *m*/*z* 556.2771 and introduced at 1 µL/min at 45 second intervals with a 3 scan average and mass window of +/- 0.5 Da. The MSe data were acquired

using two scan functions corresponding to low energy for function 1 and high energy for function 2. Function 1 had collision energy at 6 V and function 2 had a collision energy ramp of
500 18 − 42 V.

RAW MSe files were processed using Protein Lynx Global Server (PLGS) version 3.0.3 (Waters, Milford, MA). Processing parameters consisted of a low energy threshold set at 200.0 counts, an elevated energy threshold set at 25.0 counts, and an intensity threshold set at 1500 counts. Each sample was searched against the *Salpingoeca rosetta* genome hosted on
505 Ensembl Genomes [19,67]. Each databank was randomized within PLGS and included the protein sequence for ClpB. Possible structure modifications included for consideration were methionine oxidation, asparagine deamidation, glutamine deamidation, serine dehydration, threonine dehydration, and carbamidomethylation of cysteine. For viewing, PLGS search results were exported in Scaffold v4.4.6 (Proteome Software Inc., Portland, OR).

510

Generation of* Sr-p38^{T110M} *strains by genome editing

Candidate guide RNA sequences were obtained for *Sr-p38* using the EuPaGDT tool (http://grna.ctegd.uga.edu/) and the *S. rosetta* genome [19] hosted on Ensembl Protists (Ensembl 108) [68]. Guide RNA length was set at 15 and an NGG PAM sequence was used. Guide RNA
515 candidates were filtered for guides with one on-target hit (including making sure the guides do not span exon-exon boundaries), zero off-target hits (including against the genome of the co-cultured bacterium *E. pacifica*), lowest strength of the predicted secondary structure (assessed using the RNAfold web server: http://rna.tbi.univie.ac.at/cgi-bin/RNAWebSuite/RNAfold.cgi), and annealing near codon 110 of *Sr-p38*. A crRNA with the guide sequence
520 CTACATCATCACAGAGAAGA, as well as universal tracrRNAs, were ordered from IDT (Integrated DNA Technologies, Coralville, IA). Repair templates were designed as single-

stranded DNA oligos, in the same sense strand as the guide RNA, with 50 base pairs of genomic sequence on either side of the DSB cut site. The repair oligo GGTTGACCTGTACATCTCCGACGCGCGTGACATCTACATCATCATGGAGAAGATGGTGTGT
525 ATCTTTGACGCGGGTTGACTGGCCGTGATGGCGCGTGTT

was ordered from IDT as an Ultramer. Genome editing proceeded as described previously (Coyle 2023).

Bioinformatic analysis of the* S. rosetta *kinome

530 The *S. rosetta* kinome was annotated based on previously predicted kinases [19] and orthoDB ortholog annotation [69] of *S. rosetta* and human protein sequences in Uniprot [70] (Figure S1). For prediction of choanoflagellate p38 kinases, a HMMER profile was generated from human and previously predicted *S. rosetta* p38 kinases [19,45] and searched against available genomes and transcriptomes of choanoflagellates [9,12,71,72] (Figure S6A-B). Protein targets of
535 individual human kinase inhibitors were manually annotated and plotted using CORAL [73] (Figure S1). References for kinase inhibitory data for each compound is available in Table S1. To analyze conservation within the kinase domain, kinase sequence alignments of predicted kinases were generated with Clustal Omega [74] (Figure S5B-C; Figure S9B) and amino acid logos were generated with WebLogo [75] (Figure S5A).

540

Author Contributions: F.U.N.R., M.C., A.C.D., and N.K. designed research; F.U.N.R. performed screening and choanoflagellate research, M.C. generated choanoflagellate strains, and A.P.S. synthesized sorafenib analogs; F.U.N.R., A.C.D., and N.K. analyzed data; and F.U.N.R., and N.K. wrote the paper.

545

Conflicts of Interest: There are no conflicts of interest to declare.

Data Availability: Data supporting this article are included in the Supplementary Information. Raw data for this article, including flow cytometry files, imaging output files, western blot images and quantitation, are available at Figshare at https://doi.org/10.6084/m9.figshare.20669730.v2 .

550 **Acknowledgments**

We thank D. Booth, M. Carver, A. Garcia De Las Bayonas and J. Reyes-Rivera for critical reading of the manuscript; K. Shokat (University of California, San Francisco) for the contribution of kinase inhibitors in the screened library and Shokat lab members for discussions; M. West and P. He of the High-Throughput Screening Facility (QB3 HTSF) at UC Berkeley who
555 provided access to the Agilent V11 Bravo liquid handling system for screening plate generation through funding from the National Institutes of Health (S10OD021828); H. Nolla, A. Valeros and the CRL-FACS facility and staff at UC Berkeley for their support and providing access to the BD LSRII flow cytometer and BD HTS sample loading robot; A. Andaya of the mass spectrometry facility at UC Davis. The A.C.D. laboratory receives support from the NIH (RO1s CA227636,
560 CA258736, CA256480, and R56 AG066712), the Mark Foundation for Cancer Research (20-030-ASP, 21-039-ASP) and Alex's Lemonade Stand Foundation for Childhood Cancer. N.K. and F.U.N.R.'s work was supported by an Investigator award (N.K.) and the Hanna H. Gray Fellows Program (F.U.N.R.), both from the Howard Hughes Medical Institute.

565

570 **References**

1 P. Avasthi, A. Marley, H. Lin, E. Gregori-Puigjane, B. K. Shoichet, M. von Zastrow and W. F. Marshall, A chemical screen identifies class a G-protein coupled receptors as regulators of cilia, *ACS Chem. Biol.*, 2012, **7**, 911–919.

575 2 T. U. Mayer, T. M. Kapoor, S. J. Haggarty, R. W. King, S. L. Schreiber and T. J. Mitchison, Small molecule inhibitor of mitotic spindle bipolarity identified in a phenotype-based screen, *Science*, 1999, **286**, 971–974.

3 J. R. Peterson and T. J. Mitchison, Small molecules, big impact: a history of chemical inhibitors and the cytoskeleton, *Chem. Biol.*, 2002, **9**, 1275–1285.

580 4 D. P. Walsh and Y.-T. Chang, Chemical genetics, *Chem. Rev.*, 2006, **106**, 2476–2530.

5 P. Blume-Jensen and T. Hunter, Oncogenic kinase signalling, *Nature*, 2001, **411**, 355–365.

6 M. A. Lemmon and J. Schlessinger, Cell signaling by receptor tyrosine kinases, *Cell*, 2010, **141**, 1117–1134.

7 R. Roskoski Jr, Properties of FDA-approved small molecule protein kinase inhibitors: A
585 2024 update, *Pharmacol. Res.*, 2024, **200**, 107059.

8 G. Manning, S. L. Young, W. T. Miller and Y. Zhai, The protist, Monosiga brevicollis, has a tyrosine kinase signaling network more elaborate and diverse than found in any known metazoan, *Proc. Natl. Acad. Sci. U. S. A.*, 2008, **105**, 9674–9679.

9 N. King, M. J. Westbrook, S. L. Young, A. Kuo, M. Abedin, J. Chapman, S. Fairclough, U.
590 Hellsten, Y. Isogai, I. Letunic, M. Marr, D. Pincus, N. Putnam, A. Rokas, K. J. Wright, R. Zuzow, W. Dirks, M. Good, D. Goodstein, D. Lemons, W. Li, J. B. Lyons, A. Morris, S. Nichols, D. J. Richter, A. Salamov, J. G. I. Sequencing, P. Bork, W. A. Lim, G. Manning, W. T. Miller, W. McGinnis, H. Shapiro, R. Tjian, I. V. Grigoriev and D. Rokhsar, The genome of the choanoflagellate Monosiga brevicollis and the origin of metazoans, *Nature*, 2008, **451**,
595 783–788.

10 W. Yeung, A. Kwon, R. Taujale, C. Bunn, A. Venkat and N. Kannan, Evolution of Functional Diversity in the Holozoan Tyrosine Kinome, *Mol. Biol. Evol.*, 2021, **38**, 5625–5639.

11 N. Ros-Rocher, A. Pérez-Posada, M. M. Leger and I. Ruiz-Trillo, The origin of animals: an ancestral reconstruction of the unicellular-to-multicellular transition, *Open Biol.*, 2021, **11**,
600 200359.

12 D. J. Richter, P. Fozouni, M. B. Eisen and N. King, Gene family innovation, conservation and loss on the animal stem lineage, *Elife*, 2018, **7**, e34226.

13 D. S. Booth and N. King, Genome editing enables reverse genetics of multicellular development in the choanoflagellate Salpingoeca rosetta, *Elife*, , DOI:10.7554/eLife.56193.

605 14 M. A. Shogren-Knaak, P. J. Alaimo and K. M. Shokat, Recent advances in chemical approaches to the study of biological systems, *Annu. Rev. Cell Dev. Biol.*, 2001, **17**, 405–433.

15 N. King, C. T. Hittinger and S. B. Carroll, Evolution of key cell signaling and adhesion protein families predates animal origins, *Science*, 2003, **301**, 361–363.

610 16 R. Bertrand, E. Solary, P. O'Connor, K. W. Kohn and Y. Pommier, Induction of a common pathway of apoptosis by staurosporine, *Exp. Cell Res.*, 1994, **211**, 314–321.

17 M. Deponte, Programmed cell death in protists, *Biochim. Biophys. Acta*, 2008, **1783**, 1396–1405.

18 J. H. Zhang, T. D. Chung and K. R. Oldenburg, A simple statistical parameter for use in
615 evaluation and validation of high throughput screening assays, *J. Biomol. Screen.*, 1999, **4**, 67–73.

19 S. R. Fairclough, Z. Chen, E. Kramer, Q. Zeng, S. Young, H. M. Robertson, E. Begovic, D. J. Richter, C. Russ, M. J. Westbrook, G. Manning, B. F. Lang, B. Haas, C. Nusbaum and N. King, Premetazoan genome evolution and the regulation of cell differentiation in the choanoflagellate Salpingoeca rosetta, *Genome Biol.*, 2013, **14**, R15.
20 T. J. P. van Dam, F. J. T. Zwartkruis, J. L. Bos and B. Snel, Evolution of the TOR pathway, *J. Mol. Evol.*, 2011, **73**, 209–220.
21 M. Belenky, J. Prasain, H. Kim and S. Barnes, DING, a genistein target in human breast cancer: a protein without a gene, *J. Nutr.*, 2003, **133**, 2497S-2501S.
22 Z.-C. Dang, V. Audinot, S. E. Papapoulos, J. A. Boutin and C. W. G. M. Löwik, Peroxisome proliferator-activated receptor gamma (PPARgamma) as a molecular target for the soy phytoestrogen genistein, *J. Biol. Chem.*, 2003, **278**, 962–967.
23 J. B. Müller, P. E. Geyer, A. R. Colaço, P. V. Treit, M. T. Strauss, M. Oroshi, S. Doll, S. Virreira Winter, J. M. Bader, N. Köhler, F. Theis, A. Santos and M. Mann, The proteome landscape of the kingdoms of life, *Nature*, 2020, **582**, 592–596.
24 J. Reinders and A. Sickmann, State-of-the-art in phosphoproteomics, *Proteomics*, 2005, **5**, 4052–4061.
25 M. Mann, S. E. Ong, M. Grønborg, H. Steen, O. N. Jensen and A. Pandey, Analysis of protein phosphorylation using mass spectrometry: deciphering the phosphoproteome, *Trends Biotechnol.*, 2002, **20**, 261–268.
26 B. M. Sefton and S. Shenolikar, Overview of protein phosphorylation, *Curr. Protoc. Protein Sci.*, 2001, **Chapter 13**, Unit13.1.
27 Y. Segawa, H. Suga, N. Iwabe, C. Oneyama, T. Akagi, T. Miyata and M. Okada, Functional development of Src tyrosine kinases during evolution from a unicellular ancestor to multicellular animals, *Proc. Natl. Acad. Sci. U. S. A.*, 2006, **103**, 12021–12026.
28 W. Li, S. L. Young, N. King and W. T. Miller, Signaling properties of a non-metazoan Src kinase and the evolutionary history of Src negative regulation, *J. Biol. Chem.*, 2008, **283**, 15491–15501.
29 K. P. Schultheiss, B. P. Craddock, M. Tong, M. Seeliger and W. T. Miller, Metazoan-like signaling in a unicellular receptor tyrosine kinase, *BMC Biochem.*, 2013, **14**, 4.
30 S. U. Aleem, B. P. Craddock and W. T. Miller, Constitutive Activity in an Ancestral Form of Abl Tyrosine Kinase, *PLoS One*, 2015, **10**, e0131062.
31 S. H. Myers, V. G. Brunton and A. Unciti-Broceta, AXL inhibitors in cancer: A medicinal chemistry perspective, *J. Med. Chem.*, 2016, **59**, 3593–3608.
32 M. I. Davis, J. P. Hunt, S. Herrgard, P. Ciceri, L. M. Wodicka, G. Pallares, M. Hocker, D. K. Treiber and P. P. Zarrinkar, Comprehensive analysis of kinase inhibitor selectivity, *Nat. Biotechnol.*, 2011, **29**, 1046–1051.
33 B. Apsel, J. A. Blair, B. Gonzalez, T. M. Nazif, M. E. Feldman, B. Aizenstein, R. Hoffman, R. L. Williams, K. M. Shokat and Z. A. Knight, Targeted polypharmacology: discovery of dual inhibitors of tyrosine and phosphoinositide kinases, *Nat. Chem. Biol.*, 2008, **4**, 691–699.
34 M. S. Lopez, J. W. Choy, U. Peters, M. L. Sos, D. O. Morgan and K. M. Shokat, Staurosporine-derived inhibitors broaden the scope of analog-sensitive kinase technology, *J. Am. Chem. Soc.*, 2013, **135**, 18153–18159.
35 S. S. Taylor, M. M. Keshwani, J. M. Steichen and A. P. Kornev, Evolution of the eukaryotic protein kinases as dynamic molecular switches, *Philos. Trans. R. Soc. Lond. B Biol. Sci.*, 2012, **367**, 2517–2528.
36 J. A. Adams, Kinetic and catalytic mechanisms of protein kinases, *Chem. Rev.*, 2001, **101**, 2271–2290.

37 G. Manning, D. B. Whyte, R. Martinez, T. Hunter and S. Sudarsanam, The protein kinase complement of the human genome, *Science*, 2002, **298**, 1912–1934.
38 Y. Liu, A. Bishop, L. Witucki, B. Kraybill, E. Shimizu, J. Tsien, J. Ubersax, J. Blethrow, D. O. Morgan and K. M. Shokat, Structural basis for selective inhibition of Src family kinases by PP1, *Chem. Biol.*, 1999, **6**, 671–678.
39 C. Zhang, M. S. Lopez, A. C. Dar, E. Ladow, S. Finkbeiner, C.-H. Yun, M. J. Eck and K. M. Shokat, Structure-guided inhibitor design expands the scope of analog-sensitive kinase technology, *ACS Chem. Biol.*, 2013, **8**, 1931–1938.
40 J. G. Villamor, F. Kaschani, T. Colby, J. Oeljeklaus, D. Zhao, M. Kaiser, M. P. Patricelli and R. A. L. van der Hoorn, Profiling protein kinases and other ATP binding proteins in Arabidopsis using Acyl-ATP probes, *Mol. Cell. Proteomics*, 2013, **12**, 2481–2496.
41 M. P. Patricelli, A. K. Szardenings, M. Liyanage, T. K. Nomanbhoy, M. Wu, H. Weissig, A. Aban, D. Chun, S. Tanner and J. W. Kozarich, Functional interrogation of the kinome using nucleotide acyl phosphates, *Biochemistry*, 2007, **46**, 350–358.
42 J. C. Silva, M. V. Gorenstein, G.-Z. Li, J. P. C. Vissers and S. J. Geromanos, Absolute Quantification of Proteins by LCMSE, *Molecular & Cellular Proteomics*, 2006, **5**, 144–156.
43 R. Rudalska, D. Dauch, T. Longerich, K. McJunkin, T. Wuestefeld, T.-W. Kang, A. Hohmeyer, M. Pesic, J. Leibold, A. von Thun, P. Schirmacher, J. Zuber, K.-H. Weiss, S. Powers, N. P. Malek, M. Eilers, B. Sipos, S. W. Lowe, R. Geffers, S. Laufer and L. Zender, In vivo RNAi screening identifies a mechanism of sorafenib resistance in liver cancer, *Nat. Med.*, 2014, **20**, 1138–1146.
44 J. X. Yu, A. J. Craig, M. E. Duffy, C. Villacorta-Martin, V. Miguela, M. Ruiz de Galarreta, A. P. Scopton, L. Silber, A. Y. Maldonado, A. Rialdi, E. Guccione, A. Lujambio, A. Villanueva and A. C. Dar, Phenotype-Based Screens with Conformation-Specific Inhibitors Reveal p38 Gamma and Delta as Targets for HCC Polypharmacology, *Mol. Cancer Ther.*, 2019, **18**, 1506–1519.
45 V. Shabardina, P. R. Charria, G. B. Saborido, E. Diaz-Mora, A. Cuenda, I. Ruiz-Trillo and J. J. Sanz-Ezquerro, Evolutionary analysis of p38 stress-activated kinases in unicellular relatives of animals suggests an ancestral function in osmotic stress, *Open Biol.*, 2023, **13**, 220314.
46 J. L. Brewster, T. de Valoir, N. D. Dwyer, E. Winter and M. C. Gustin, An osmosensing signal transduction pathway in yeast, *Science*, 1993, **259**, 1760–1763.
47 J. L. Brewster and M. C. Gustin, Hog1: 20 years of discovery and impact, *Sci. Signal.*, 2014, **7**, re7.
48 H. C. Causton, B. Ren, S. S. Koh, C. T. Harbison, E. Kanin, E. G. Jennings, T. I. Lee, H. L. True, E. S. Lander and R. A. Young, Remodeling of yeast genome expression in response to environmental changes, *Mol. Biol. Cell*, 2001, **12**, 323–337.
49 C. Schüller, J. L. Brewster, M. R. Alexander, M. C. Gustin and H. Ruis, The HOG pathway controls osmotic regulation of transcription via the stress response element (STRE) of the Saccharomyces cerevisiae CTT1 gene, *EMBO J.*, 1994, **13**, 4382–4389.
50 A. Cuadrado and A. R. Nebreda, Mechanisms and functions of p38 MAPK signalling, *Biochem. J.*, 2010, **429**, 403–417.
51 S. Dorion, H. Lambert and J. Landry, Activation of the p38 signaling pathway by heat shock involves the dissociation of glutathione S-transferase Mu from Ask1, *J. Biol. Chem.*, 2002, **277**, 30792–30797.
52 J. Rouse, P. Cohen, S. Trigon, M. Morange, A. Alonso-Llamazares, D. Zamanillo, T. Hunt and A. R. Nebreda, A novel kinase cascade triggered by stress and heat shock that stimulates MAPKAP kinase-2 and phosphorylation of the small heat shock proteins, *Cell*, 1994, **78**, 1027–1037.

53 M. Carr, B. S. C. Leadbeater, R. Hassan, M. Nelson and S. L. Baldauf, Molecular phylogeny of choanoflagellates, the sister group to Metazoa, *Proc. Natl. Acad. Sci. U. S. A.*, 2008, **105**, 16641–16646.
54 B. S. C. Leadbeater, *The Choanoflagellates*, Cambridge University Press, 2015.
55 L. Tomanek, Variation in the heat shock response and its implication for predicting the effect of global climate change on species' biogeographical distribution ranges and metabolic costs, *J. Exp. Biol.*, 2010, **213**, 971–979.
56 Y. Jiang, C. Chen, Z. Li, W. Guo, J. A. Gegner, S. Lin and J. Han, Characterization of the structure and function of a new mitogen-activated protein kinase (p38β), *Journal of Biological*, 1996, **271**, 17920–17926.
57 Y. Devary, R. A. Gottlieb, T. Smeal and M. Karin, The mammalian ultraviolet response is triggered by activation of Src tyrosine kinases, *Cell*, 1992, **71**, 1081–1091.
58 M. Sonoshita, A. P. Scopton, P. M. U. Ung, M. A. Murray, L. Silber, A. Y. Maldonado, A. Real, A. Schlessinger, R. L. Cagan and A. C. Dar, A whole-animal platform to advance a clinical kinase inhibitor into new disease space, *Nat. Chem. Biol.*, 2018, **14**, 291–298.
59 S. J. Dixon, D. N. Patel, M. Welsch, R. Skouta, E. D. Lee, M. Hayano, A. G. Thomas, C. E. Gleason, N. P. Tatonetti, B. S. Slusher and B. R. Stockwell, Pharmacological inhibition of cystine-glutamate exchange induces endoplasmic reticulum stress and ferroptosis, *Elife*, 2014, **3**, e02523.
60 H. Suga, M. Dacre, A. de Mendoza, K. Shalchian-Tabrizi, G. Manning and I. Ruiz-Trillo, Genomic Survey of Premetazoans Shows Deep Conservation of Cytoplasmic Tyrosine Kinases and Multiple Radiations of Receptor Tyrosine Kinases, *Science Signaling*, 2012, **5**, ra35.
61 W. A. Weiss, S. S. Taylor and K. M. Shokat, Recognizing and exploiting differences between RNAi and small-molecule inhibitors, *Nat. Chem. Biol.*, 2007, **3**, 739–744.
62 N. King, S. L. Young, M. Abedin, M. Carr and B. S. C. Leadbeater, Starting and maintaining Monosiga brevicollis cultures, *Cold Spring Harb. Protoc.*, 2009, **2009**, db.prot5148.
63 T. C. Levin and N. King, Evidence for sex and recombination in the choanoflagellate Salpingoeca rosetta, *Curr. Biol.*, 2013, **23**, 2176–2180.
64 A. Woznica, A. M. Cantley, C. Beemelmanns, E. Freinkman, J. Clardy and N. King, Bacterial lipids activate, synergize, and inhibit a developmental switch in choanoflagellates, *Proc. Natl. Acad. Sci. U. S. A.*, 2016, **113**, 7894–7899.
65 A. C. Dar, T. K. Das, K. M. Shokat and R. L. Cagan, Chemical genetic discovery of targets and anti-targets for cancer polypharmacology, *Nature*, 2012, **486**, 80–84.
66 M. A. Sigg, T. Menchen, C. Lee, J. Johnson, M. K. Jungnickel, S. P. Choksi, G. Garcia 3rd, H. Busengdal, G. W. Dougherty, P. Pennekamp, C. Werner, F. Rentzsch, H. M. Florman, N. Krogan, J. B. Wallingford, H. Omran and J. F. Reiter, Evolutionary Proteomics Uncovers Ancient Associations of Cilia with Signaling Pathways, *Dev. Cell*, 2017, **43**, 744-762.e11.
67 A. D. Yates, J. Allen, R. M. Amode, A. G. Azov, M. Barba, A. Becerra, J. Bhai, L. I. Campbell, M. Carbajo Martinez, M. Chakiachvili, K. Chougule, M. Christensen, B. Contreras-Moreira, A. Cuzick, L. Da Rin Fioretto, P. Davis, N. H. De Silva, S. Diamantakis, S. Dyer, J. Elser, C. V. Filippi, A. Gall, D. Grigoriadis, C. Guijarro-Clarke, P. Gupta, K. E. Hammond-Kosack, K. L. Howe, P. Jaiswal, V. Kaikala, V. Kumar, S. Kumari, N. Langridge, T. Le, M. Luypaert, G. L. Maslen, T. Maurel, B. Moore, M. Muffato, A. Mushtaq, G. Naamati, S. Naithani, A. Olson, A. Parker, M. Paulini, H. Pedro, E. Perry, J. Preece, M. Quinton-Tulloch, F. Rodgers, M. Rosello, M. Ruffier, J. Seager, V. Sitnik, M. Szpak, J. Tate, M. K. Tello-Ruiz, S. J. Trevanion, M. Urban, D. Ware, S. Wei, G. Williams, A. Winterbottom, M. Zarowiecki, R. D. Finn and P. Flicek, Ensembl Genomes 2022: an expanding genome resource for non-vertebrates, *Nucleic Acids Res.*, 2022, **50**, D996–D1003.

68 F. Cunningham, J. E. Allen, J. Allen, J. Alvarez-Jarreta, M. R. Amode, I. M. Armean, O. Austine-Orimoloye, A. G. Azov, I. Barnes, R. Bennett, A. Berry, J. Bhai, A. Bignell, K. Billis, S. Boddu, L. Brooks, M. Charkhchi, C. Cummins, L. Da Rin Fioretto, C. Davidson, K. Dodiya, S. Donaldson, B. El Houdaigui, T. El Naboulsi, R. Fatima, C. G. Giron, T. Genez, J. G. Martinez, C. Guijarro-Clarke, A. Gymer, M. Hardy, Z. Hollis, T. Hourlier, T. Hunt, T. Juettemann, V. Kaikala, M. Kay, I. Lavidas, T. Le, D. Lemos, J. C. Marugán, S. Mohanan, A. Mushtaq, M. Naven, D. N. Ogeh, A. Parker, A. Parton, M. Perry, I. Piližota, I. Prosovetskaia, M. P. Sakthivel, A. I. A. Salam, B. M. Schmitt, H. Schuilenburg, D. Sheppard, J. G. Pérez-Silva, W. Stark, E. Steed, K. Sutinen, R. Sukumaran, D. Sumathipala, M.-M. Suner, M. Szpak, A. Thormann, F. F. Tricomi, D. Urbina-Gómez, A. Veidenberg, T. A. Walsh, B. Walts, N. Willhoft, A. Winterbottom, E. Wass, M. Chakiachvili, B. Flint, A. Frankish, S. Giorgetti, L. Haggerty, S. E. Hunt, G. R. Ilsley, J. E. Loveland, F. J. Martin, B. Moore, J. M. Mudge, M. Muffato, E. Perry, M. Ruffier, J. Tate, D. Thybert, S. J. Trevanion, S. Dyer, P. W. Harrison, K. L. Howe, A. D. Yates, D. R. Zerbino and P. Flicek, Ensembl 2022, *Nucleic Acids Res.*, 2022, **50**, D988–D995.

69 E. M. Zdobnov, D. Kuznetsov, F. Tegenfeldt, M. Manni, M. Berkeley and E. V. Kriventseva, OrthoDB in 2020: evolutionary and functional annotations of orthologs, *Nucleic Acids Res.*, 2021, **49**, D389–D393.

70 The UniProt Consortium, UniProt: the universal protein knowledgebase in 2021, *Nucleic Acids Res.*, 2021, **49**, D480–D489.

71 T. Brunet, B. T. Larson, T. A. Linden, M. J. A. Vermeij, K. McDonald and N. King, Light-regulated collective contractility in a multicellular choanoflagellate, *Science*, 2019, **366**, 326–334.

72 D. M. Needham, S. Yoshizawa, T. Hosaka, C. Poirier, C. J. Choi, E. Hehenberger, N. A. T. Irwin, S. Wilken, C.-M. Yung, C. Bachy, R. Kurihara, Y. Nakajima, K. Kojima, T. Kimura-Someya, G. Leonard, R. R. Malmstrom, D. R. Mende, D. K. Olson, Y. Sudo, S. Sudek, T. A. Richards, E. F. DeLong, P. J. Keeling, A. E. Santoro, M. Shirouzu, W. Iwasaki and A. Z. Worden, A distinct lineage of giant viruses brings a rhodopsin photosystem to unicellular marine predators, *Proc. Natl. Acad. Sci. U. S. A.*, 2019, **116**, 20574–20583.

73 K. S. Metz, E. M. Deoudes, M. E. Berginski, I. Jimenez-Ruiz, B. A. Aksoy, J. Hammerbacher, S. M. Gomez and D. H. Phanstiel, Coral: Clear and Customizable Visualization of Human Kinome Data, *Cell Syst*, 2018, **7**, 347-350.e1.

74 F. Madeira, M. Pearce, A. R. N. Tivey, P. Basutkar, J. Lee, O. Edbali, N. Madhusoodanan, A. Kolesnikov and R. Lopez, Search and sequence analysis tools services from EMBL-EBI in 2022, *Nucleic Acids Res.*, , DOI:10.1093/nar/gkac240.

75 G. E. Crooks, G. Hon, J.-M. Chandonia and S. E. Brenner, WebLogo: a sequence logo generator, *Genome Res.*, 2004, **14**, 1188–1190.

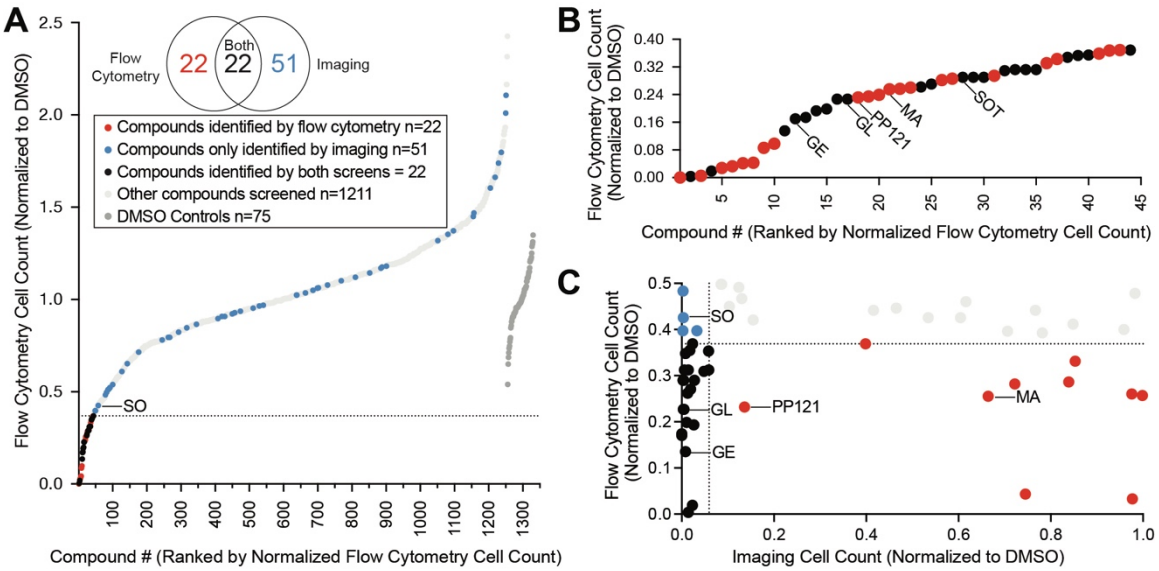

Figure 1. High-throughput screening of a small molecule library revealed inhibitors of *S. rosetta* cell proliferation. (A) Treatment of *S. rosetta* cultures with 1255 different small molecules (see Table S1 for the list of compounds, cell counts, and annotated human kinase targets) resulted in a distribution of cell counts, assessed by flow cytometry, at the 24-hour endpoint. *S. rosetta* cell counts were normalized to DMSO controls (dark grey). Compounds determined to significantly inhibit *S. rosetta* cell proliferation (based on two-tailed p-value < 0.05 calculated from z-score) are indicated in red, compounds that were not detected as significant inhibitors by flow cytometry but were identified by imaging (based on two-tailed p-value < 0.05 calculated from z-score) are in blue and compounds that were not significant inhibitors for either screen are indicated in light grey. Z-score statistics of the assays are indicated in Figure S2B and Figure S2E. Sorafenib (SO), the focus of this study, is labeled. (B) The range of normalized cell counts for compounds that significantly inhibited *S. rosetta* cell proliferation by flow cytometry. Compounds that were the focus of further study – genistein (GE), glesatinib (GL), PP121, masitinib (MA), sotrastaurin (SOT) – are labeled. Z-score statistics of the assays are indicated in Figure S2B. (C) Comparison of normalized values of compounds that inhibited *S. rosetta* cell proliferation, assessed by flow cytometry and their corresponding normalized values by imaging. Compounds that were the focus of further study – sorafenib (SO), genistein (GE), glesatinib (GL), PP121, masitinib (MA) – are labeled.

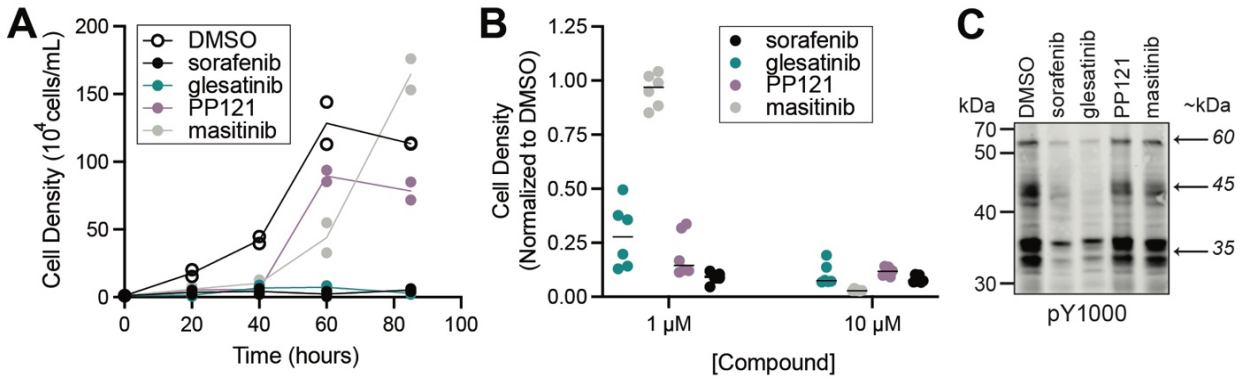

Figure 2. Glesatinib and sorafenib, two multi-target tyrosine kinase inhibitors, disrupt *S. rosetta* cell proliferation and tyrosine phosphosignaling. (A) Treatment of *S. rosetta* cultures with 1 μM sorafenib and glesatinib led to a complete block of cell proliferation, while treatment with 1 μM masitinib or PP121 led to a partial reduction in cell proliferation relative to DMSO-treated cultures. Two biological replicates were conducted per treatment, and each point represents the mean of three measurements from each biological replicate. For timepoints at 40, 60, and 85 hours, cell densities of inhibitor-treated cultures were significantly different from vehicle (DMSO) (p-value <0.01). Significance was determined by a two-way ANOVA multiple comparisons test. (B) *S. rosetta* cultures treated with 1 μM or 10 μM sorafenib, glesatinib, or PP121 for 24 hours had reduced normalized cell density, whereas masitinib only had reduced normalized cell density at 10 μM. Normalized cell densities were determined to be reduced if differences between treatments and vehicle (DMSO) were significant (p-value <0.01) Significance was determined by determined by a two-way ANOVA multiple comparisons test. Movies show *S. rosetta* cells treated with 10 μM glesatinib that undergo cell lysis (Movie S1) and sorafenib, that have cell body deformation (Movies S2-S3), in comparison to DMSO control (Movie S4). (C) Western blot analysis of *S. rosetta* cultures treated with 1 μM sorafenib and glesatinib for 1 hour showed a decrease in tyrosine phosphorylation of proteins at ~60kDa, ~45kDa, and ~35kDa (indicated by arrows and detected with pY1000 anti-phosphotyrosine antibody) compared to vehicle (DMSO) control. Masitinib and PP121 did not reduce the phosphotyrosine signal.

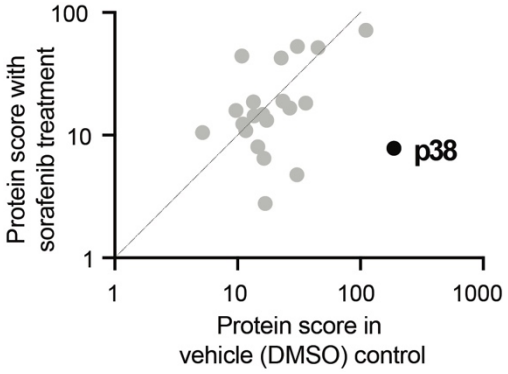

850

Figure 3. *S. rosetta* p38 binds to Sorafenib. The ActivX ATP probe was used to pull down kinases from *S. rosetta* lysates that were pretreated with either DMSO or the ATP-competitive inhibitor sorafenib. We found that pretreatment with sorafenib reduced the level of p38 recovered using the ActivX ATP probe, indicating that sorafenib and p38 interact and
855 outcompete ActivX ATP probe binding. Kinases plotted are only those that were identified in both vehicle and sorafenib pre-treatments. For full kinase enrichment list, see Table S2, and for alignment of *S. rosetta* p38 with those from animals and fungi, see Fig. S9.

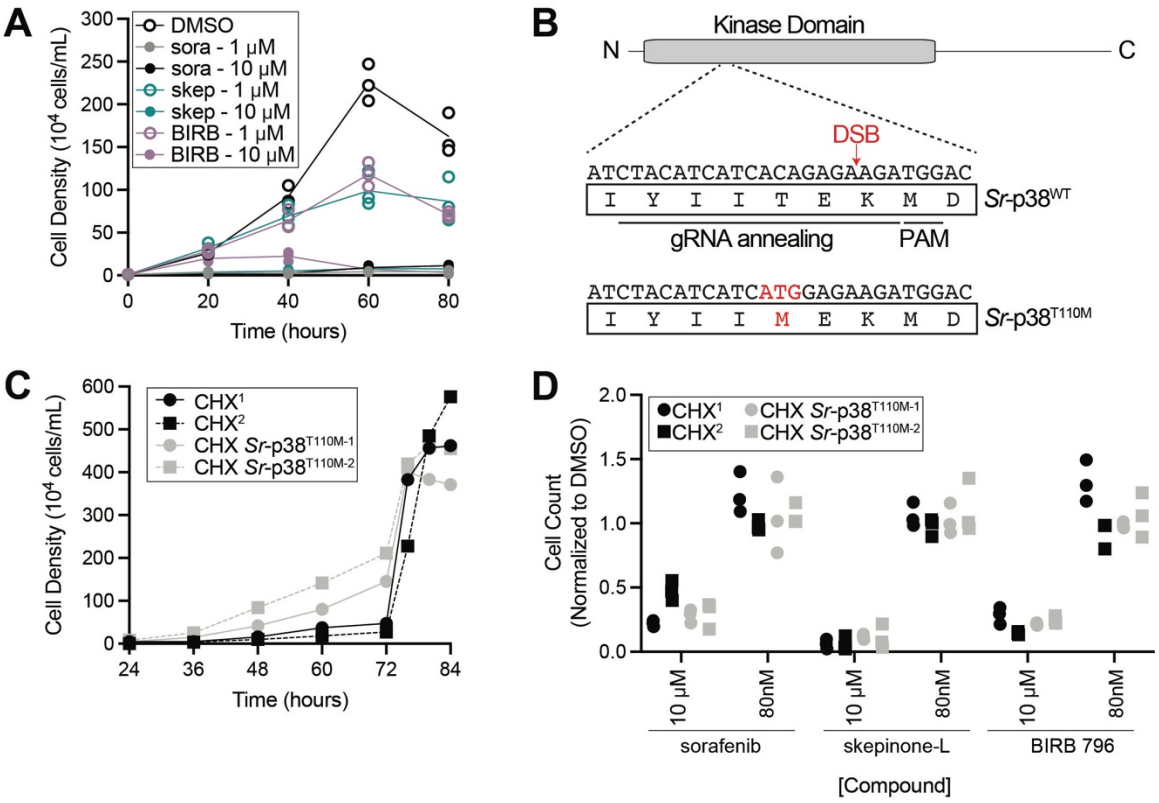

Figure 4. Inhibitors of human p38 kinases disrupt *S. rosetta* cell proliferation through multiple kinase targets. (A) Human p38 kinase inhibitors disrupt *S. rosetta* cell proliferation. *S. rosetta* cultures were treated with sorafenib or one of two human p38-specific inhibitors, skepinone-L or BIRB 796, in 24-well plates over an 80-hour growth course. At 40 hours, cells treated with 10 μM skepinone-L, BIRB 796 or sorafenib showed little evidence of cell proliferation in comparison to vehicle (DMSO) control (p-value <0.01). Cells treated with 1 μM skepinone-L or BIRB 796 had reduced cell density in comparison to vehicle (DMSO) control (p-value <0.01) at 60 hours. Three biological replicates were conducted per experiment and significance was determined by determined by a two-way ANOVA multiple comparisons test. (B) Strategy for generating Sr-p38^{T110M} cell lines. The *S. rosetta* p38 locus was targeted by a guide RNA complexed with Cas9 that anneals near the "gatekeeper" amino acid codon 110 in the kinase domain and directs Cas9 to introduce a double-strand break (DSB) downstream of codon 110. The Cas9-guide RNA complex was coupled with a homology-directed repair template to insert a cassette that encodes a threonine to methionine mutation at position 110. In humans, this mutation desensitizes p38 to sorafenib, and skepinone-L [44]. (C) Two independent clones maintained with cycloheximide (CHX) resistance, CHX Sr-p38$^{T110M-1}$, and CHX Sr-p38$^{T110M-2}$, do not show a growth defect when compared CHX^1 and CHX^2, two strains that are only cycloheximide-resistant. Three technical replicates were conducted per strain, and significance was determined by a two-way ANOVA multiple comparisons test. (D) CHX Sr-p38^{T110M} strains do not show decreased sensitivity to human p38 kinase inhibitors. Two independent CHX Sr-p38^{T110M} and CHX strains were treated with sorafenib, skepinone-L, and BIRB 796, and cells were counted after 24 hours. Normalized counts did not differ between the

treated CHX Sr-p38^{T110M} and CHX strains. Three technical replicates were conducted per strain, and significance was determined by a two-way ANOVA multiple comparisons test.

885

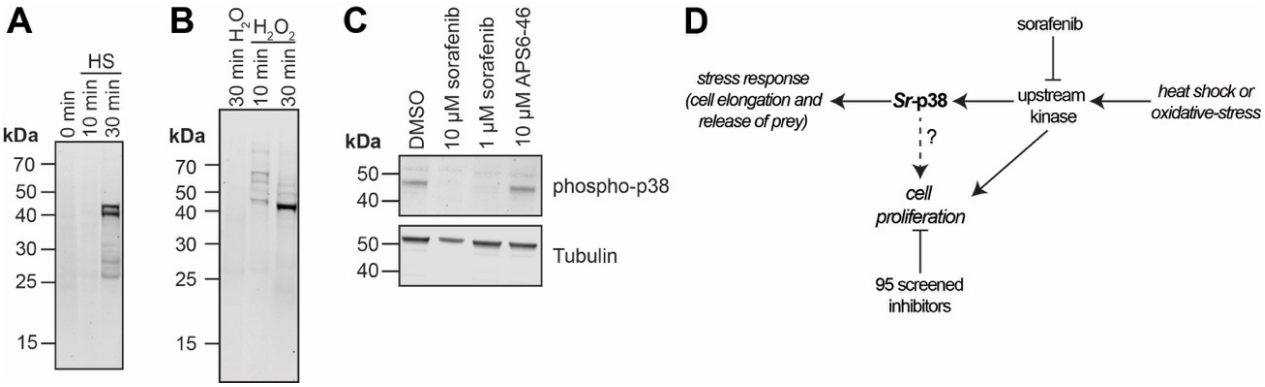

Figure 5. *S. rosetta* p38 signaling is activated by environmental stressors and inhibited by sorafenib. *S. rosetta* cells, normally cultured at 22°C were incubated at 37°C or treated with hydrogen peroxide to induce heat shock or oxidative stress for 10 min. and 30 min. Lysates
890 from the treated cultures were analyzed by western blot with an antibody specific for phosphorylated p38 kinase (phospho-p38) to identify if any changes in *Sr*-p38 phosphorylation occurred. (A) 30 minutes of heat shock was sufficient to induce *Sr*-p38 phosphorylation as was (B) 10 min of treatment with 0.5M H_2O_2 at 22°C. (C) The induction of *Sr*-p38 phosphorylation by heat shock was kinase-dependent. *S. rosetta* cultures pretreated with 10 µM or 1 µM sorafenib
895 for 30 minutes followed by 30 minutes of heat shock at 37°C had decreased *Sr*-p38 phosphorylation. APS6-46 treated cultures were not different from vehicle (DMSO) control. 4-12% Bis-Tris SDS-PAGE gels were used to resolve the western bands observed. An anisomycin-treated human cell lysate was used as a positive control to validate the anti-phospho-p38 antibody in Figure S8C. (D) Proposed mechanism for regulation of the stress-
900 responsive *Sr*-p38 axis. *Sr*-p38 is phosphorylated by upstream kinases in response to heat shock and oxidative stress. Sorafenib, a multi-kinase inhibitor, targets kinases upstream of *Sr*-p38 and disrupts *Sr*-p38 signaling. Skepinone-L and BIRB 796, two selective human p38 inhibitors, disrupt S. rosetta cell proliferation independent of *Sr*-p38 signaling.